RSC Advances

COMMUNICATION

View Article Online
View Journal | View Issue

Cite this: *RSC Adv.*, 2015, **5**, 63271

Received 23rd April 2015
Accepted 6th July 2015

DOI: 10.1039/c5ra07390a

www.rsc.org/advances

Feasibility tests of $-SO_3H/-SO_3^-$-functionalized magnesium phyllosilicate [$-SO_3H/-SO_3^-$ MP] for environmental and bioenergy applications

Hyun Gu Kang,†[a] Kyoung Min Lee,†[a] Saehae Choi,[b] Bora Nam,[c] Sun-A Choi,[c] Soon-Chang Lee,[d] Ji-Yeon Park,[c] Go-Woon Lee,[e] Hyun Uk Lee*[f] and Young-Chul Lee*[a]

We have prepared a simple water-solubilized, transparent, and anionic clay. –SH-functionalized magnesium phyllosilicate [–SH MP] was easily oxidized into $-SO_3H/-SO_3^-$-functionalized magnesium phyllosilicate [$-SO_3H/-SO_3^-$ MP] by treatment of 5.0% H_2O_2 at 60 °C for 24 hours, showing a pH of ~2.0. These water-solubilized and anionic nanoparticles (NPs) were tested with organo-building blocks of $-SO_3H/-SO_3^-$ MP for removal of cationic pollutant dye (methylene blue) and heavy metals (Cd^{2+} and Pb^{2+}). Furthermore, interactions of ubiquitous humic acid (HA) with $-SO_3H/-SO_3^-$ MP were removed due to an ion exchange mechanism. For bioenergy applications, glucose conversion from cellulose was tested, focusing on Brønsted acid-rich sites in $-SO_3H/-SO_3^-$ MP.

Introduction

Organic–inorganic building-block behaviors in aqueous solution have emerged in the self-assembly of nano-objects or patterns, which induces wrapping or precipitation systems in bionanotechnology[1,2] and environmental engineering.[3,4] Recently, among diverse phyllosilicate clays, the sol–gel-organized phyllosilicate family has emerged as a hot topic due to the high density of primary amines (*i.e.*, aminoclays)[5,6] or thiol organic pendants (*i.e.*, –SH MP),[7,8] mass-produced under ambient conditions by a simple one-pot method.[9] Specifically, water-solubilized and cationic-zeta-potential aminoclays among the phyllosilicate family,[10,11] showing homogeneous nanoparticles (NPs) in aqueous solution,[12] can effectively interact with negatively charged target molecules, ions or other particles, generally within a few minutes.[13,14] As another phyllosilicate clay, –SH MP has provided higher removal capacities for heavy metals,[7,8] but it was not both water-solubilized and acting as an organo-building block. It is indicated that the interaction of certain (nano)materials with oppositely charged anionic organo-building blocks of phyllosilicate clays has yet to be reported, due to the absence of directly utilized and proper organosilane precursors. If developed, water-solubilized (water dispersible) and anionic phyllosilicate clays,[12,13,15] like the previous aminoclays, are also expected to have useful applications in the (bio)energy, environmental, and medical fields.

Herein a two step synthesis phyllosilicate clay is reported. After preparation of –SH MP, a $-SO_3H/-SO_3^-$-functionalized magnesium phyllosilicate ($-SO_3H/-SO_3^-$ MP) with a pH of ~2.0 was produced by 5.0% H_2O_2 oxidation (at 60 °C for 24 hours) of the as-prepared –SH MP as a precipitate in aqueous solution. As a result, $-SO_3H/-SO_3^-$ MP with a homogenous system in aqueous solution was tested for its environmental-application feasibility for the removal of cationic methylene blue (MB), heavy metals, and ubiquitous water-soluble humic acid (HA); it was also tested as a polysaccharide hydrolysis catalyst for its bioenergy-application potential with respect to its glucose production from two types of cellulose using abundant Brønsted acid sites.

Materials and methods

Synthesis of the $-SO_3H/-SO_3^-$ MP solution

Prior to preparation of $-SO_3H/-SO_3^-$ MP, –SH MP was synthesized following the procedure available in the literature.[1,7,8,16] Briefly, 8.4 g of $MgCl_2 \cdot 6H_2O$ salt (Jusei, Japan) was dissolved into a 200 mL ethanol solution and stirred for 10 min. Then, 1.3 mL of (3-mercaptopropyl)trimethoxysilane (MTES) (Sigma-

[a]*Department of BioNano Technology, Gachon University, 1342 Seongnamdaero, Sujeong-gu, Seongnam-si, Gyeonggi-do 461-701, Republic of Korea. E-mail: dreamdbs@gachon.ac.kr*

[b]*Sustainable Bioresource Research Center, Korea Research Institute of Bioscience & Biotechnology (KRIBB), Daejeon 305-806, Republic of Korea*

[c]*Biomass and Waste Energy Laboratory, Korea Institute of Energy Research (KIER), 152 Gajeong-ro, Yuseong-gu, Daejeon 305-343, Republic of Korea*

[d]*Department of Fine Chemical Engineering and Applied Chemistry, Chungnam National University, Daejeon 305-764, Republic of Korea*

[e]*Quality Management Team, Korea Institute of Energy Research (KIER), 152 Gajeong-ro, Yuseong-gu, Daejeon 305-343, Republic of Korea*

[f]*Advanced Nano-Surface Research Group, Korea Basic Science Institute (KBSI), Daejeon 305-333, Republic of Korea. E-mail: leeho@kbsi.re.kr*

† These authors contributed equally to this work.

Aldrich, USA) was added, followed immediately by 10 mL of 5.0 M NaOH solution (Daejung, Korea) to induce the sol–gel reaction under ambient conditions.[16] After 24 hours of reaction, a white slurry was produced. After 6000 × *g* centrifugation for 10 min, ethanol washings were performed 2 times. A 24-hour drying process in a 60 °C oven was conducted to evaporate the remaining ethanol to obtain the –SH MP sample. Subsequently, the sample was powdered again using a pestle and mortar. Finally, 0.2 g of –SH MP was dispersed in 30 mL Teflon-coated polypropylene (PP) bottles containing 18 mL of deionized water, to which 3.5 wt% and 5.0 wt% H_2O_2 concentrations were adjusted.[17] The solutions were then hydrothermally treated at 60 °C for 24 hours to induce –SH oxidation and ultimately produce $-SO_3H/-SO_3^-$ MP.

Morphological observations of the as-prepared –SH and $-SO_3H/-SO_3^-$ MP using electron microscopy (EM)

1.0 mg mL^{-1} of –SH MP or $-SO_3H/-SO_3^-$ MP in aqueous solution was dropped onto a carbon-coated copper grid on paper tissue (KIMTECH, Yuhan-Kimberly, Korea) to adsorb water in the sample, which was then examined using 200 kV transmission electron microscopy (TEM, Tecnai F20model, Netherlands)

For only cellulose and $-SO_3H/-SO_3^-$ MP-treated cellulose, the sample was dropped onto tape and examined using cold-type field-emission scanning electron microscopy (FE-SEM, SEM-4700) at 0.5–30 V and 1 pA^{-2} nA as well as elemental X-ray analysis (EDX) in the 4 Be–92 U range.[3]

Characterization of $-SO_3H/-SO_3^-$ MP using spectroscopic methods

For confirmation of the crystalline structure and impurities in the –SH powder and $-SO_3H/-SO_3^-$ film MP, micro-area X-ray diffractometry (D/MAX-2500, RIGAKU) and multi-purpose thin-film X-ray diffractometry (D/MAX-2500, RIGAKU) with normal scan mode at 40 kV and 300 mA were performed from 3° to 70° in 0.01 step size increments and at a rate of 3° min^{-1}, respectively. In order to check the covalent bonding between organic groups in –SH and $-SO_3H/-SO_3^-$ MP, the Fourier transform infrared (FT-IR) spectra were recorded using FT-IR spectrometry (FT-IR 4100, Jasco, Japan), prior to which the FT-IR sample was prepared with KBr (90 wt%) and –SH or $-SO_3H/-SO_3^-$ MP (10 wt%). For analysis of the elemental-composition and chemical binding species of the $-SO_3H/-SO_3^-$ MP surface, high-resolution X-ray photoelectron spectroscopy (HR-XPS) utilizing monochromatic Al Kα X-ray radiation at a power of 120 W (Kratos Analytical, AXIS Nova, UK) was employed. For $-SO_3H/-SO_3^-$ MP, the shift in the binding energy (eV) due to relative surface charging was corrected and the curves were fitted, based on an internal standard (the C1s level at 284.69 eV). For confirmation of the condensation degree of Si in the $-SO_3H/-SO_3^-$ MP sample, a ^{29}Si cross polarization (CP) magic angle spinning (MAS) 500 MHz liquid nuclear magnetic resonance (NMR) spectrometer (Agilent, VNMRS) was operated at room temperature using tetramethylsilane (TMS) as the reference sample and D_2O as the solvent.

Other characterizations of $-SO_3H/-SO_3^-$ MP

Samples were analyzed for hydrodynamic size and zeta potential in aqueous solution using dynamic light scattering (DLS) methods (Zeta-sizer Nano ZS, Malvern, UK). Elemental analysis (EA) of the sulfur (S) composition (%) and X-ray fluorescence (XRF) analysis of the silicon (Si) composition (%) in the –SH MP powder were performed using an elemental analysis analyzer (EA1108 and NA2000, CE Instruments, USA). Also, the silicon (Si) concentration (mg L^{-1}) at 11.11 mg mL^{-1} of the $-SO_3H/-SO_3^-$ MP solution was measured using inductively coupled plasma atomic emission spectroscopy (ICP-AES, Varian, USA). The sample pH was measured with a pH/ion meter (D-53, Horiba, Kyoto, Japan).

Experimental methylene blue (MB), heavy metal (Cd^{2+} and Pb^{2+}) and humic acid (HA) removal

The cationic dye (methylene blue, MB) was calibrated at 664 nm, resulting in an MB concentration of 0–5.0 mg L^{-1} with <1.0 absorbance intensity. At 2 mg L^{-1} of 20 mL MB and according to the $-SO_3H/-SO_3^-$ MP concentrations (1.11, 3.33, 5.55, 8.88, and 11.11 mg mL^{-1}), MB-removal experiments were performed using UV-vis spectrophotometry (Varian, Cary 5000) at the temperature of 18 ± 2 °C.

For heavy-metal (Cd^{2+} and Pb^{2+})-removal testing, 30 mg L^{-1} of both cadmium chloride ($CdCl_2$, Sigma-Aldrich, USA) and lead chloride ($PbCl_2$, Sigma-Aldrich, USA) were mixed in 1.11 mg mL^{-1} of $SO_3H/-SO_3^-$ MP kinetically. The heavy metals were analyzed with a permeate solution using a 0.1 μm syringe filter (Sartorius, Germany) and inductively coupled plasma atomic emission spectroscopy (ICP-AES, Varian, USA). Experiments were performed in duplicate, and the results were averaged.[4]

Likewise, for humic acid (HA)-removal testing, 100 mg L^{-1} of HA was mixed with various $-SO_3H/-SO_3^-$ MP concentrations (1.67, 2.22, and 2.78 mg mL^{-1}). Then, after having been left to stand for 30 min, tests using survey scanning in UV-vis spectrophotometry (Varian, Cary 5000) were conducted for supernatant solutions at the temperature of 18 ± 2 °C.

Experimental hydrolysis of cellulose using $-SO_3H/-SO_3^-$ MP

0.2 g of α-cellulose (Sigma-Aldrich, USA) and microcrystalline cellulose (Sigma-Aldrich, USA) in 200 mg of $-SO_3H/-SO_3^-$ MP in an 18 mL water solution (11.11 mg mL^{-1}) were prepared in Teflon-coated polypropylene (PP) bottles. According to the temperature (100, 120, and 150 °C) and hydrothermally autoclaved time (6, 12, and 24 hours), the solutions were tested. After filtering with a 0.1 μm syringe (Sartorius, Germany), high-performance liquid chromatography (HPLC) was performed. The HPLC system (Shimadzu Co., Japan), incorporating a Bio-Rad Aminex HPX-87H analytical column (300 mm × 7.8 mm) and a Cation H microguard cartridge (30 mm × 4.6 mm) (Bio-Rad Laboratories Inc., Hercules, CA) was used for carbohydrate measurement. The column, maintained at 60 °C with 5 mmol L^{-1} H_2SO_4 eluent (flow rate: 0.6 mL min^{-1}), allows for concurrent analysis of acetic and formic acids as well as glucose. The sugar peaks were detected using a RI detector

(Shimadzu Co., Japan) and identified and quantified by comparison with the retention times of authentic standards.[18] Data were averaged with three runs using repeated experimental samples.

Results and discussion

Preparation of –SO_3H/–SO_3^- MP

In Fig. 1a (top panel), schematic pictures of the as-prepared –SH MP conversion to –SO_3H/–SO_3^- MP by 3.5% H_2O_2 oxidation *via* partial delamination of –SH MP then full 5.0% H_2O_2 oxidation of –SO_3H/–SO_3^- MP is depicted, corresponding to the digital camera images and transmission electron microscopy (TEM) micrographs in the bottom panel (Fig. 1b). The color of –SH MP in aqueous solution is opaque but after the full 5.0% H_2O_2 oxidation of –SH MP to –SO_3H/–SO_3^- MP the solution displayed a transparent and homogenous condition *via* the translucent state of –SO_3H/–SO_3^- MP by 3.5% H_2O_2 oxidation of –SH MP. The morphology of –SH MP exhibited layer-stacked sheets of a clay structure, which was in good agreement with previous reports on the phyllosilicate family.[5,7,8] However, morphological alternation with a fractal-like tree structure, by partial delamination of electrostatic repulsion between the clay sheets, was observed. Under 5.0% H_2O_2 oxidation, the process afforded well-dispersed organo-building blocks of –SO_3H/–SO_3^- MPof 20–200 nm in diameter.

Spectroscopic characterizations

–SH and –SO_3H/–SO_3^- MP spectral characterizations are shown in Fig. 2. For confirmation of the crystalline structure and identification of –SH and –SO_3H/–SO_3^- MP, Fig. 2a presents that –SH MP displayed the 2 : 1 trioctahedral smectite structure at $2\theta = \sim 60^\circ$ of the $d_{060,330}$ plane. Notably, the mesolamellar-layered distinct peak of the d_{001} spacing with 1.25 nm at $2\theta = 7.09^\circ$ in the inset of Fig. 2a disappeared after oxidation of the –SH groups to –SO_3H/–SO_3^- ones. The mesolamellar peak in –SO_3H/–SO_3^- MP disappeared due to the random distribution of the organo-building blocks. The disappearance of the *d*-spacing at the (001) plane in –SO_3H/–SO_3^- MP was sometimes observed for the re-assembly of the organo-building blocks of aminoclay,[19] with the typical amorphous phyllosilicate clay structure at $2\theta = 9.55^\circ$ at d_{002} and 21.62° at $d_{020,110}$ and a weak intensity of $2\theta = 35.26^\circ$ at $d_{130,200}$ in –SO_3H/–SO_3^- MP.[7,8] Moreover, the broad in-plane peaks at d_{002}, $d_{020,110}$, and $d_{130,200}$ in –SH MP matched well with talc-like phyllosilicate, this result is in good agreement with the literature.[5,7,8] In Fig. 2b, covalent bonding in –SH MP revealed (ν-OH) at 3423 cm^{-1}, (ν-CH_2–) at 2920 and 2850 cm^{-1}, (δ-OH) at 1656 cm^{-1}, (νSi–C) at 1145 cm^{-1}, (νSi–O–Si) at 1,035 cm^{-1}, (νC–S) at 693 cm^{-1}, and (νMg–O) at 605 cm^{-1}, corresponding with the previous data.[8] Although the vibration peak of the –SH-functional group at ~2550 cm^{-1} was not found in this study,[8] however, most of the vibration peaks matched with those of –SH MP. For the vibration peaks in –SO_3H/–SO_3^- MP, those of the –SO_3H/–SO_3^- functional groups were indicated in the 1340 cm^{-1}–1030 cm^{-1} range, in particular 1196 cm^{-1} of the –SO_2 stretching mode and 1044 cm^{-1} of the

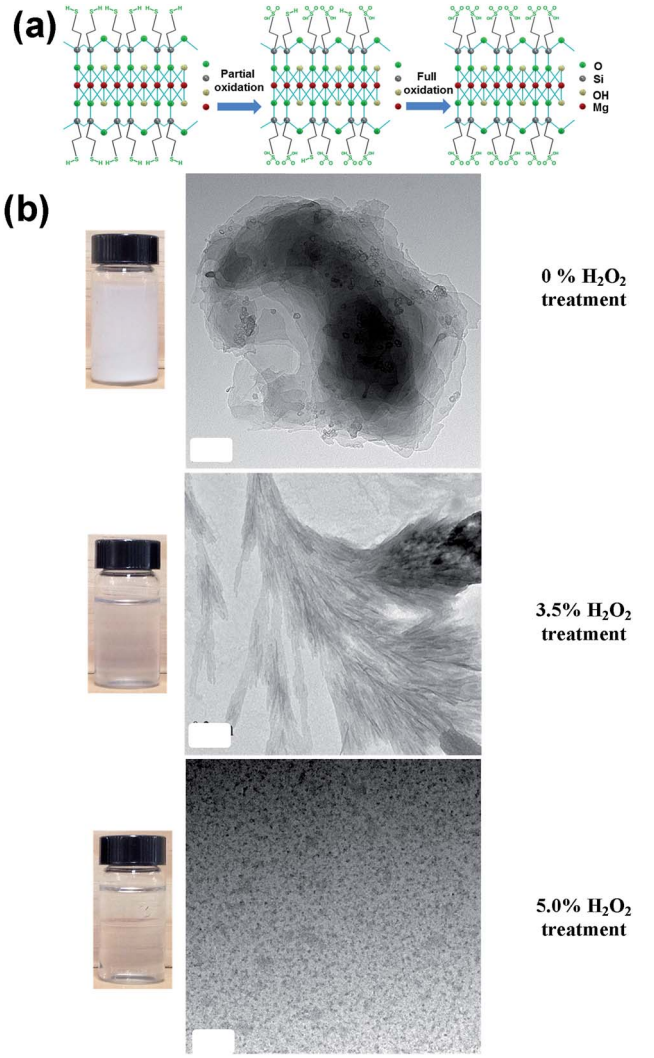

Fig. 1 Schematic representation of the formation of –SO_3H/–SO_3^- MP organo-building-block clusters by oxidation of –SH MP. Top panels (a): Approximate unit structure of Mg-phyllosilicate clay according to different concentrations of H_2O_2 oxidation. Bottom panels (b): Corresponding digital camera image of glass vials at 11.11 mg mL^{-1} (left) and transmission electron microscopy (TEM) (right) images of respective 0%, 3.5%, and 5.0% H_2O_2 treatment of –SH MP in dispersed water (1.0 mg mL^{-1}). Scale bars are the white boxes in the TEM images = 200 nm.

–SO_3^- stretching mode in –SO_3H groups.[20,21] Focusing on the –SO_3H/–SO_3^- species, XPS survey scans detected O_{1s} at 532.41 eV, C_{1s} at 284.69 eV, S_{2s} at 233.89 eV, and S_{2p} at 170.49 eV (Fig. 2c). Fig. 2d shows 169.87 eV at S_{2p^1} and 168.7 eV at S_{2p^3} in –SO_3H and 167.6 eV at S_{2p^1} and 166.5 eV at S_{2p^3} in –SO_3^-, and further weak curves 167.65 eV at S_{2p^1} and 166.5 eV at S_{2p^3} in –SH with 0.04 and 0.09 relative area ratios when divided by S_{2p^3} in –SO_3H.[20,21] This indicated that –SH MP was successfully oxidized to –SO_3H/–SO_3^- MP, leading to anionic charged organo-building blocks in –SO_3H/–SO_3^- MP which were delaminated in aqueous solution by repulsion interactions. Additionally, elemental analysis (EA) revealed the sulfur (S) composition to be ~10.7% (~3.34 mmol g^{-1}). The Si

concentration using the XRF technique was measured to be ~27.4% (~9.78 mmol g^{-1}), indicating that the Si/S ratio is ~2.9. The Si concentration of the $-SO_3H/-SO_3^-$ MP solution at 11.11 mg mL^{-1} was confirmed by ICP-AES measurements, resulting in ~2.054 mg mL^{-1}. The degree of Si condensation in $-SO_3H/-SO_3^-$ MP was tested by obtaining a ^{29}Si-MAS-NMR spectrum of $-SO_3H/-SO_3^-$ MP. It shows three signals at −49/−59, −55 to −58/−70, and −67/−78 ppm associated with R–SiO–$(OH)_2$ (T1 signal), R–SiO_2–OH (T2 signal), and R–SiO_3– (T3/Q3 signal) in the inorganic–organic backbone structure of $-SO_3H/-SO_3^-$ MP, displaying almost complete condensation of MTES, confirmed by a dominant T3 signal (data not shown).[22]

Environmental application

Using water-solubilized $-SO_3H/-SO_3^-$ MP, methylene blue (MB) as a cationic dye model was tested for removal kinetics in the electrostatic attraction between $-SO_3H/-SO_3^-$ MP and cationic dyes as well as the ion exchange process between protons in $-SO_3H/-SO_3^-$ MP, inducing MB removal. Fig. 3a indicates that 1.11 mg mL^{-1} of $-SO_3H/-SO_3^-$ MP showed a transparent property ranging from 200 nm to 700 nm wavelengths with lower absorbance intensities. The relative absorbance intensity in the UV range is related to the residual H_2O_2 in the $-SO_3H/-SO_3^-$ MP solution. As the $-SO_3H/-SO_3^-$ MP concentrations were increased, the absorbance of MB decreased as a result of adsorption or precipitation by $-SO_3H/-SO_3^-$ MP within 10 min, due to the electrostatic attraction and ion exchange process between MB molecules and the organo-building blocks of $-SO_3H/-SO_3^-$ MP; this compares with only 2 mg L^{-1} of MB at a shoulder peak of ~614 nm and a strong visible peak of 664 nm, which was in line with the photographs of discoloration in 2 mg L^{-1} of MB (Fig. 3b). Further, heavy metal (Cd^{2+} and Pb^{2+}) removal by $-SO_3H/-SO_3^-$ MP at pH ~4.0 was applied kinetically (Fig. 3c). Within 5 min, fast removal efficiencies were achieved. For the removal of 30 mg L^{-1} Cd^{2+} and Pb^{2+} by 11.11 mg mL^{-1} of $-SO_3H/-SO_3^-$ MP, 0.81 and 1.35 mg g^{-1} (heavy metal per $-SO_3H/-SO_3^-$ MP) removal capacities in a homogenous system were achieved. The removal rates of heavy metals (Cd^{2+} and Pb^{2+}) by $-SO_3H/-SO_3^-$ MP were 2.959×10^{-3} and 7.925×10^{-3} min^{-1}, respectively. This fast-removal phenomenon is similar to oxyanion removal by water-soluble aminoclay.[4] Taking into consideration the real practical environment, ubiquitous organic matter can affect the heavy metal removal behavior of the $-SO_3H/-SO_3^-$ MP colloidal solutions. Fig. 3d exhibits the interaction of water-soluble humic acid (HA) according to $-SO_3H/-SO_3^-$ MP concentrations. With increased $-SO_3H/-SO_3^-$ MP concentrations, HA removal occurred by the ion exchange mechanism and a decrease of HA solubility in aqueous solution was due to a decrease in pH as well as electrostatic interactions with microenvironmental sites in the macromolecular HA.[23] In the inset of Fig. 3d, it can be seen that the brown-colored HA in the supernatant solution became transparent after precipitation. At 100 mg L^{-1} of HA, 2.78 mg mL^{-1} of $-SO_3H/-SO_3^-$ MP showed a ~98% decrease of turbidity within 30 min. Cationic amine groups in macromolecular HA can mainly interact with $-SO_3H/-SO_3^-$ MP or the ion exchange driving force. Generally, in the presence of organic matter, heavy-metal removal by $-SO_3H/-SO_3^-$ MP was not inhibited, because HA, simultaneously, also played a role in the removal of heavy metals.[4]

Bioenergy application

To test the bioenergy application of water-solubilized and Brønsted acid-rich $-SO_3H/-SO_3^-$ MP, glucose production from α-cellulose and microcrystalline cellulose under hydrolysis according to hydrothermal temperatures (100, 120, and 150 °C) and auto-clave times (6, 12, and 24 h) was evaluated. The averaged product yields from high-performance liquid chromatography (HPLC) analysis are summarized in Table 1. Under the 150 °C and 12 h conditions, the highest glucose production yields, 0.850 g L^{-1} and 1.066 g L^{-1} for 10 g L^{-1} of respective α-cellulose and microcrystalline cellulose in aqueous solution, were obtained. The higher glucose yield for microcrystalline cellulose than that for α-cellulose is attributable to the finer powder (*i.e.*, smaller particle size with higher surface area) affording easier access to polysaccharide hydrolysis contacting sites in the catalytic functionalities. Under the optimal hydrothermal auto-claved treatment of microcrystalline cellulose, formic acid and acetic acid (g L^{-1}) were produced, as by-products *via* glucose intermediates, in 1.213 and 1.039 g L^{-1} yields, respectively, in particular these amounts were nearly equivalent to those of glucose.

Fig. 4 shows the surface-morphological alterations of cellulose after hydrolysis with $-SO_3H/-SO_3^-$ MP treatment. Smooth pristine α-cellulose surfaces (Fig. 4a and b) were changed to rough surfaces with many holes after hydrolysis by 11.11 mg mL^{-1} of $-SO_3H/-SO_3^-$ MP treatment for 11.11 mg mL^{-1} of α-cellulose (Fig. 4c and d).[24,25] Note that the red-dotted rectangular boxes can be easily discerned in Fig. 4a–d.

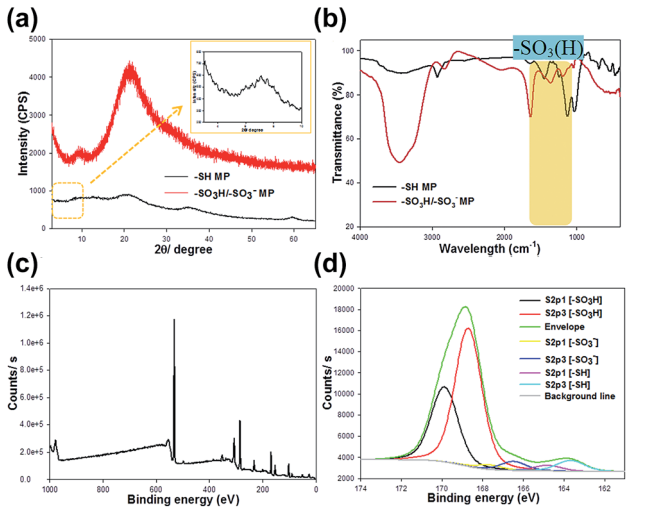

Fig. 2 (a) X-ray diffraction (XRD) pattern of −SH and $-SO_3H/-SO_3^-$ MP where the inset shows the diffraction pattern at a low angle of 2θ for −SH MP, (b) pellet-mode Fourier transform infrared (FT-IR) spectrum of −SH and $-SO_3H/-SO_3^-$ MP, (c) X-ray spectroscopy (XPS) survey scan spectrum of $-SO_3H/-SO_3^-$ MP, and (d) fitting curves of the S_{2p} core in the $-SO_3H/-SO_3^-$ MP XPS spectrum.

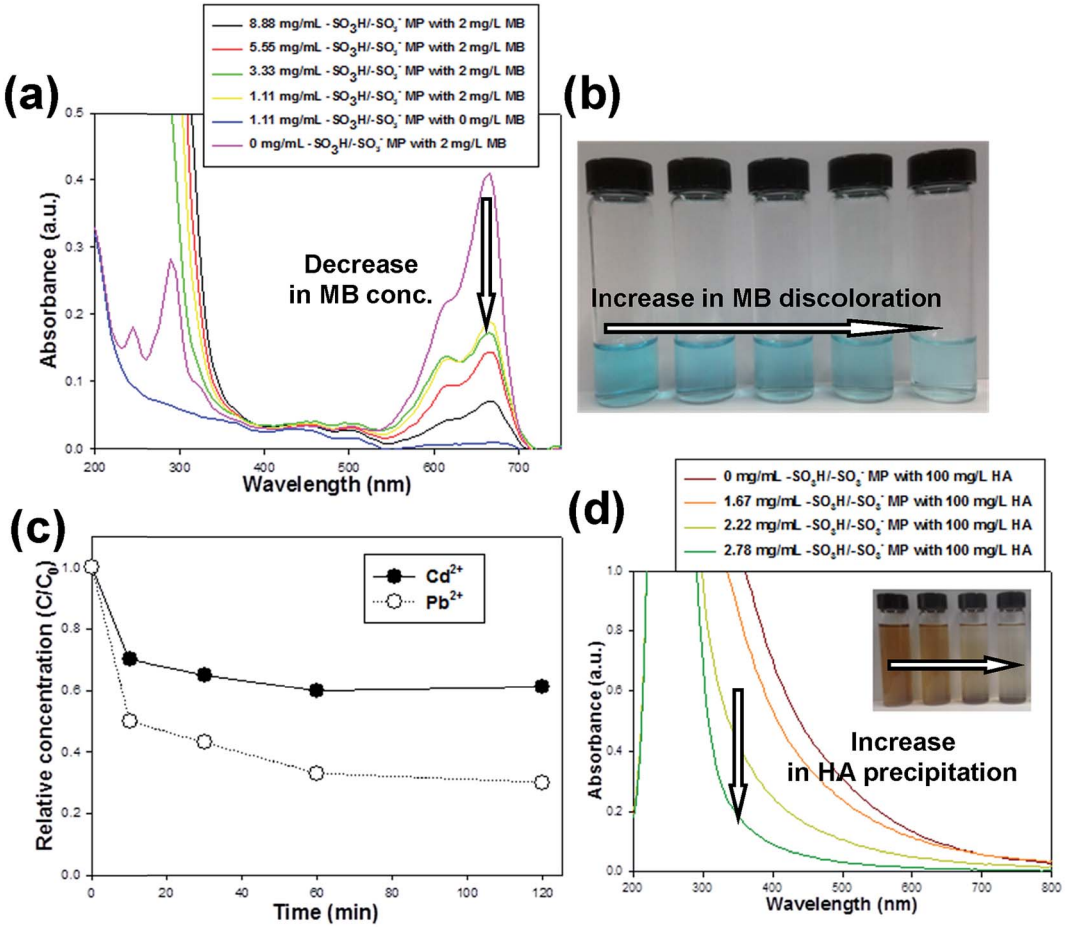

Fig. 3 (a) UV-vis absorbance spectra of 2 mg L^{-1} MB concentration according to $-SO_3H/-SO_3^-$ MP loadings, (b) its digital camera photograph, (c) heavy-metal removal kinetics of 11.11 mg mL^{-1} of $-SO_3H/-SO_3^-$ MP, and (d) UV-vis absorbance spectra of 100 mg L^{-1} HA according to $-SO_3H/-SO_3^-$ MP loadings, where the inset shows its digital camera photograph.

Table 1 Hydrolysis of cellulose by $-SO_3H/-SO_3^-$ MP[a]

Cellulose type	Temperature (°C)	Time (hour)	Glucose (g L^{-1})	Formic acid (g L^{-1})	Acetic acid (g L^{-1})
α-Cellulose	100	6	0.135	—	—
		12	0.142	—	—
		24	0.136	—	—
	120	6	0.210	—	—
		12	0.378	—	—
		24	0.288	—	—
	150	6	0.364	1.230	0.962
		12	0.850	1.579	1.015
		24	0.725	1.803	1.195
Microcrystalline cellulose	100	6	0.310	—	—
		12	0.278	—	—
		24	0.361	—	—
	120	6	0.290	—	—
		12	0.353	—	—
		24	0.465	—	—
	150	6	0.306	0.854	0.899
		12	1.066	1.213	1.039
		24	1.054	1.677	1.167

[a] Note that the — symbol indicates "not measured".

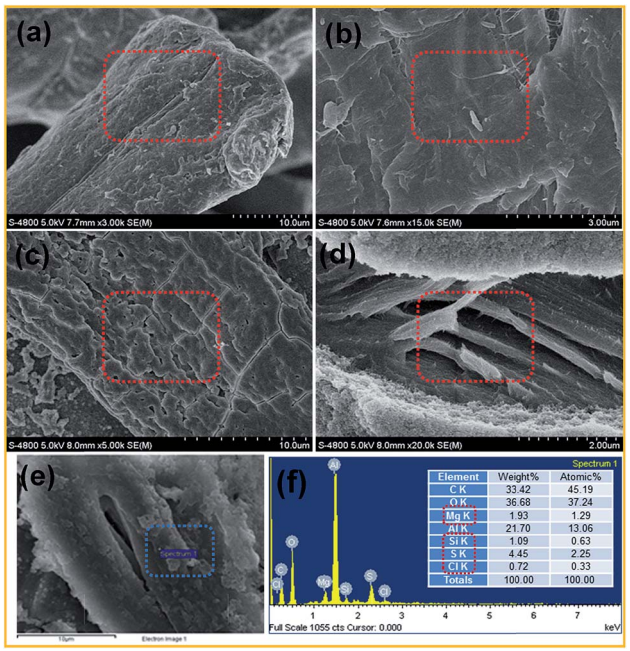

Fig. 4 Scanning electron microscopy (SEM) images and elemental-composition analysis after $-SO_3H/-SO_3^-$ MP treatment with α-cellulose: (a and b) original α-cellulose; (c and d) α-cellulose by $-SO_3H/-SO_3^-$ MP treatment; (e) α-cellulose by $-SO_3H/-SO_3^-$ MP treatment and (f) its energy-dispersive X-ray (EDX) analysis for the selected area of (e). In (f), note that the dotted red box indicates the presence of $-SO_3H/-SO_3^-$ MP in the dotted blue box in (e).

Hydrolysis occurred gradually from the outside to the inside of α-cellulose with accessible Brønsted acid-rich $-SO_3H/-SO_3^-$ MP.[20,26] The surface charge of $-SO_3H/-SO_3^-$ MP was measured as ~−8.65 mV of the zeta potential value. For the mixture of α-cellulose and $-SO_3H/-SO_3^-$ MP in aqueous solution, the zeta potential was ~−0.0654 mV. After α-cellulose hydrolysis treatment at 150 °C and 12 hours with $-SO_3H/-SO_3^-$ MP, the hydrodynamic size of the α-cellulose with $-SO_3H/-SO_3^-$ shrunk from ~25.14 μm to ~14.69 μm. Fig. 4e shows the $-SO_3H/-SO_3^-$ MP coated on the hydrolyzed α-cellulose surface. The presence of C and O in the elemental-composition analysis (Fig. 4f) is sourced from both the α-cellulose and $-SO_3H/-SO_3^-$ MP, while the Mg, Si, S, and Cl compositions indicate the presence of $-SO_3H/-SO_3^-$ MP, because in the absence of $-SO_3H/-SO_3^-$ MP, compositions of Mg, Si, S, and Cl were not detected in only α-cellulose. Thus, it is believed that $-SO_3H/-SO_3^-$ MP is a potential heterogeneous catalyst for the hydrolysis of polysaccharides. The, immobilization of mechanically and thermally stabilized $-SO_3H/-SO_3^-$ MP onto macro-sized matrixes is suggested as a practical commercial means of facile catalyst recovery.

Conclusions

In summary, we developed water-solubilized and anionic magnesium phyllosilicate [$-SO_3H/-SO_3^-$ MP] with pH ~2.0. The homogeneity of this clay in aqueous solution enabled fast removal of cationic dye, heavy metals, and HA, making this material a novel adsorbent for environmental engineering applications. Additionally, Brønsted acid-rich $-SO_3H/-SO_3^-$ MP showed potential as a hydrolysis catalyst for glucose conversion from cellulose using hydrothermal autoclaved treatment, yielding approximately ~10% glucose production at 150 °C and 12 h. We are currently pursuing the means of utilization of this water-solubilized and anionic clay in the following applications: as an electrolyte in washing agents for electrokinetic (EK) remediation of heavy-metal-contaminated soils; as a Nafion® membrane composite for direct methanol fuel cells (DMFCs), and as a self-assembled biomass-conversion catalyst with dual acidity/basicity by mixing two water-solubilized clays containing $-SO_3H/-SO_3^-$ and $-NH_2/-NH_3^+$ organo-functional groups, *i.e.*, combination of two-dimensional materials with unique properties.

Acknowledgements

This subject is supported by the Korea Ministry of Environment as "The GAIA project" and by Gachon University's Cube Research Program of Creative Korea (CK); it as also supported by the New & Renewable Energy Technology Development Program of the Korea Institute of Energy Technology Evaluation and Planning (KETEP) funded by the Korean Ministry of Knowledge Economy (No. 20123010090010).

Notes and references

1 S. Mann, *Nat. Mater.*, 2009, **8**, 781–792.
2 A. J. Patil and S. Mann, *J. Mater. Chem.*, 2008, **18**, 4605–4615.
3 Y.-C. Lee, S.-J. Jang, M.-H. Choi, T.-J. Jeon, T. Ryu and Y. S. Huh, *Appl. Catal., B*, 2013, **142–143**, 494–503.
4 Y.-C. Lee, W.-K. Park and J.-W. Yang, *J. Hazard. Mater.*, 2011, **190**, 652–658.
5 S. Mann, S. L. Burkett, S. A. Davis, C. E. Fowler, N. H. Mendelson, S. D. Sims, D. Walsh and N. T. Whilton, *Chem. Mater.*, 1997, **9**, 2300–2310.
6 K. K. R. Datta, A. Achari and M. Eswaramoorthy, *J. Mater. Chem. A*, 2013, **1**, 6707–6718.
7 M. G. Fonseca and C. Airoldi, *Thermochim. Acta*, 2000, **359**, 1–9.
8 I. Lagadic, M. K. Mitchell and B. D. Payne, *Environ. Sci. Technol.*, 2001, **35**, 984–990.
9 Y.-C. Lee, E. S. Jin, S. W. Jung, Y.-M. Kim, K. S. Chang, J.-W. Yang, S.-W. Kim, Y.-O. Kim and H.-J. Shin, *Sci. Rep.*, 2013, **3**(1–8), 1292.
10 P. Chaturbedy, D. Jagadeesan and M. Eswaramoorthy, *ACS Nano*, 2010, **4**, 5921–5929.
11 K. K. R. Datta, C. Kulkarni and M. Eswaramoorthy, *Chem. Commun.*, 2010, **46**, 616–618.
12 K. K. R. Datta, M. Eswaramoorthy and C. N. R. Rao, *J. Mater. Chem.*, 2007, **17**, 613–615.
13 Y.-C. Lee, E. J. Kim, D. A. Ko and J.-W. Yang, *J. Hazard. Mater.*, 2011, **196**, 101–108.
14 Y. Hwang, Y.-C. Lee, P. D. Mines, Y. S. Huh and H. R. Andersen, *Appl. Catal., B*, 2014, **147**, 748–755.

15 A. Achari, K. K. R. Datta, M. De, V. P. Dravid and M. Eswaramoorthy, *Nanoscale*, 2013, **5**, 5316–5320.
16 S. L. Burkett, A. Press and S. Mann, *Chem. Mater.*, 1997, **9**, 1071–1073.
17 C. H. Rhee, H. K. Kim, H. C. Chang and J. S. Lee, *Chem. Mater.*, 2005, **17**, 1691–1697.
18 J.-Y. Park, M. Kang, J. S. Kim, J.-P. Lee, W.-I. Choi and J.-S. Lee, *Bioresour. Technol.*, 2012, **123**, 707–712.
19 A. J. Patil, E. Muthusamy and S. Mann, *J. Mater. Chem.*, 2005, **15**, 3838–3843.
20 K. Nakajima and M. Hara, *ACS Catal.*, 2012, **2**, 1296–1304.
21 R. Jia, J. Ren, X. Liu, G. Lu and Y. Wang, *J. Mater. Chem. A*, 2014, **2**, 11195–11201.
22 Y.-C. Lee, Y.-S. Choi, M. Choi, H. Yang, K. Liu and H.-J. Shin, *Appl. Clay Sci.*, 2013, **83–84**, 474–485.
23 M. Cerff, M. Morweiser, R. Dillschneider, A. Michel, K. Menzel and C. Posten, *Bioresour. Technol.*, 2012, **118**, 289–295.
24 X. Li, Y. Jiang, L. Shuai, L. Wang, L. Meng and X. Mu, *J. Mater. Chem.*, 2012, **22**, 1283–1289.
25 S. Suganuma, K. Nakajima, M. Kitano, D. Yamaguchi, H. Kato, S. Hayashi and M. Hara, *J. Am. Chem. Soc.*, 2008, **130**, 12787–12893.
26 J. A. Melero, L. F. Bautista, G. Morales, J. Iglesias and R. Sánchez-Vázquez, *Chem. Eng. J.*, 2010, **161**, 323–331.